The G Protein–Coupled Receptor GPR56 Is an Inhibitory Checkpoint for NK Cell Migration

Daniel Palacios,[*,†] Rakesh Kumar Majhi,[*,‡] Edina K. Szabo,[*,†] Dennis Clement,[*,†] Mieszko Lachota,[*,§] Herman Netskar,[*,†] Leena Penna,[¶] Silje Z. Krokeide,[*,†] Marianna Vincenti,[*,†] Lise Kveberg,[*,†,1] and Karl-Johan Malmberg[*,†,‖,1]

G protein–coupled receptors (GPCRs) represent the largest family of surface receptors and are responsible for key physiological functions, including cell growth, neurotransmission, hormone release, and cell migration. The GPCR 56 (GPR56), encoded by *ADGRG1*, is an adhesion GPCR found on diverse cell types, including neural progenitor cells, melanoma cells, and lymphocytes, such as effector memory T cells, γδ T cells, and NK cells. Using RNA-sequencing and high-resolution flow cytometry, we found that GPR56 mRNA and protein expression increased with NK cell differentiation, reaching its peak in adaptive NK cells. Small interfering RNA silencing of GPR56 led to increased spontaneous and chemokine-induced migration, suggesting that GPR56 functions as an upstream checkpoint for migration of highly differentiated NK cells. Increased NK cell migration could also be induced by agonistic stimulation of GPR56 leading to rapid internalization and deactivation of the receptor. Mechanistically, GPR56 ligation and downregulation were associated with transcriptional coactivator with PDZ-binding motif translocation to the nucleus and increased actin polymerization. Together, these data provide insights into the role of GPR56 in the migratory behavior of human NK cell subsets and may open possibilities to improve NK cell infiltration into cancer tissues by releasing a migratory checkpoint. *The Journal of Immunology*, **2024, 213: 1349–1357.**

Natural killer cells have emerged as a promising tool in cell therapy, with extensive research ongoing to maximize their potential in cancer treatment (1). This involves directing NK cells to tumors and enabling their effector functions on-site. NK cells migrate toward target tissues through interactions with the extracellular environment, facilitated by chemokine receptors, adhesion molecules, and various NK cell receptor families on their surface (2). These interactions provide multiple signals, both inhibitory and activating, that modulate their migratory properties (3). The engagement of different signaling pathways leads to cytoskeletal rearrangement, resulting in migration and the activation of effector responses, such as the release of cytotoxic granules, cytokine production, and interactions with target cells (2). Of particular importance for migration are the seven-transmembrane receptors, including chemokine receptors and GPCRs (4).

GPR56, encoded by *ADGR1*, is a multifunctional adhesion GPCR involved in a long range of biological processes, including oligodendrocyte and brain development, hematopoietic stem cell generation, myoblast fusion and muscle hypertrophy, adipogenesis, testis development, immunoregulation, and tumorigenesis (5). GPR56 is expressed on hematopoietic stem and progenitor cells (HSPCs), NK cells, and T cells, including $CD8^+$, $CD4^+$, and γδ T cells (6). In HSPCs, GPR56 has proved to be necessary to overcome proliferative stress during hematopoiesis, and its expression is reduced upon cell differentiation and lineage restriction. However, GPR56 deficiency does not affect HSPC maintenance, migration, or function in hematopoiesis (7). In $CD8^+$ T cells, GPR56 expression is increased in CMV-specific effector type $CD8^+$ T cells and correlates with the expression of CD57 and KLRG1, which define terminally differentiated cells (6). In $CD4^+$ T cells, GPR56 has been suggested as a marker to classify the more functional subset of $CD4^+$ memory

*Department of Cancer Immunology, Institute for Cancer Research, Oslo University Hospital, Oslo, Norway; †Precision Immunotherapy Alliance, University of Oslo, Oslo, Norway; ‡Center of Excellence in Cancer, Gangwal School of Medical Sciences and Technology, Mehta Family Center for Engineering in Medicine, Department of Biological Sciences and Bioengineering, IIT Kanpur, India; §Laboratory of Cellular and Genetic Therapies, Medical University of Warsaw, Warsaw, Poland; ¶Finnish Red Cross Blood Service, Research and Development, Helsinki, Finland; and ‖Centre for Infectious Medicine, Department of Medicine Huddinge, Karolinska Institutet, Sweden

[1]L.K. and K.-J.M. are colast authors.

ORCIDs: 0000-0001-6999-1349 (R.K.M.); 0000-0003-4780-5458 (E.K.S.); 0000-0003-2808-8916 (M.L.); 0000-0002-3081-9581 (H.N.); 0000-0003-4918-283X (L.P.); 0009-0002-3466-8706 (S.Z.K.); 0000-0001-5361-0185 (M.V.); 0000-0001-9308-0641 (L.K.); 0000-0002-8718-9373 (K.-J.M.).

Received for publication April 29, 2024. Accepted for publication September 2, 2024.

This work was supported by the Research Council of Norway (Norges Forskningsråd; Projects 275469 and 237579); Research Council of Norway (Norges Forskningsråd) through its Centres of Excellence scheme (Project 332727); Norwegian Cancer Society (Kreftforeningen; Projects 190386 and 223310); Ministry of Health and Care Services, The South-Eastern Norway Regional Health Authority (Helse Sør-Øst RHF; Grant 2021-073); network grant of the European Commission (H2020-MSCA-MC-ITN-765104-MATURE-NK); Knut and Alice Wallenberg Foundation (Knut och Alice Wallenbergs Stiftelse); and Swedish Foundation for Strategic Research. R.K.M. was supported by the European Union's Horizon 2020 research and innovation program under Marie Sklodowska-Curie Actions Grant 801133. This work was further supported by grants from the Swedish Research Council (223310), Swedish Children's Cancer Society (PR2020-1059), Swedish Cancer Society (Cancerfonden; 21-1793Pj), Sweden's Innovation Agency, Karolinska Institutet, and National Cancer Institute (P01 CA111412 and P009500901) (all to K.-J.M.).

The sequencing data presented in this article have been submitted to the Gene Expression Omnibus (https://www.ncbi.nlm.nih.gov/geo/query/acc.cgi?acc=GSE245690) under accession number GSE245690.

Address correspondence and reprint requests to Prof. Karl-Johan Malmberg, University of Oslo, Institute of Clinical Medicine, Oslo 0310, Norway. E-mail address: k.j.malmberg@medisin.uio.no

The online version of this article contains supplemental material.

Abbreviations used in this article: CTF, C-terminal fragment; GAIN, G protein–coupled receptor autoproteolysis-inducing; GPCR, G protein–coupled receptor; GPR56, G protein–coupled receptor 56; HSPC, hematopoietic stem and progenitor cell; NTF, N-terminal fragment; PBNK, peripheral blood NK cell; RhoA, Ras homolog family member A; ROCK, Rho-associated protein kinase; scRNAseq, single-cell RNA sequencing; siRNA, small interfering RNA; TAZ, transcriptional coactivator with PDZ-binding motif; UMAP, uniform manifold approximation and projection for dimension reduction; WGA, wheat germ agglutinin; YAP, Yes-associated protein.

This article is distributed under The American Association of Immunologists, Inc., Reuse Terms and Conditions for Author Choice articles.

Copyright © 2024 by The American Association of Immunologists, Inc. 0022-1767/24/$37.50

https://doi.org/10.4049/jimmunol.2400228

T cells based on the production of the inflammatory cytokines TNF and IFN-γ (8). GPR56 expression was also found to correlate with the expression levels of Granzyme B in $CD4^+$ and $CD8^+$ T cells (9). Furthermore, GPR56 was found to be upregulated in tumor-infiltrating lymphocytes upon TCR signaling and reduced the migratory potential of tumor-infiltrating lymphocytes in response to chemoattractants (10).

In peripheral blood NK cells (PBNKs), GPR56 is known to be expressed in $CD56^{dim}$ NK cells (11) and driven by the transcription factor Hobit (12). GPR56 expression in NK cells and overexpression in NK-92 cells showed that it negatively impacts NK cell effector functions, including target killing, degranulation, and production of inflammatory cytokines. This negative impact on function is thought to be mediated through physical association with the tetraspanin CD81 (12). However, the role of GPR56 in NK cell migration remains elusive. In this study, we report a detailed characterization of the expression of GPR56 in primary human NK cell subsets and demonstrate a potential role for GPR56 as an upstream checkpoint for spontaneous and chemokine-driven migration.

Materials and Methods

NK cell isolation

PBMCs were isolated from buffy coats harvested from healthy donors at Oslo University Hospital Blood Bank (Regional Ethics committee ID 2018/2485) by density gradient centrifugation using 50-ml SepMate tubes (STEMCELL Technologies). PBNK cells were isolated using the NK Cell Isolation Kit and autoMACS Pro Separator from Miltenyi Biotec. NK cells were cultured in complete RPMI (RPMI 1640 + L-glutamine supplemented with 10% FBS, 100 U/ml penicillin, and 100 μg/ml streptomycin from Sigma-Aldrich).

Flow and mass cytometry

For flow cytometry analysis, freshly isolated NK cells were washed and stained with Abs for 15 min using staining buffer (PBS with 2% FCS). An overview of Abs and reagents is provided in Supplemental Table I. LIVE/DEAD Aqua Dead Cell Stain (Life Technologies) was included to stain dead cells. To stain intracellular proteins for flow cytometry, we fixed cells using BD Cytofix Fixation Buffer for 10 min at 4°C and then washed with BD Perm/Wash (BD Biosciences) before staining with Abs in BD Perm/Wash buffer for 30 min at 4°C. Cells were washed twice with BD Perm/Wash buffer and resuspended in staining buffer. Flow cytometry analysis was performed on a BD LSRII flow cytometer and by FlowJo. Abs were purchased for CD56 BUV395, Granzyme B AF700, CD3 V500, CD14 V500, CD19 V500, and IFN-γ allophycocyanin from BD Biosciences; CD56 ECD, KIR2DL2/S2/L3 PE-Cy5.5, and NKG2A allophycocyanin from Beckman Coulter Life Sciences; CD57 FITC, CD107 AF488, KIR3DL1 BV421 and BV711, GPR56 PE, GPR56 unconjugated, and LFA1 PE from BioLegend; and KIR2DL1 allophycocyanin-Vio 770 and KIR2DL1/S1 PE-Vio770 from Miltenyi Biotec.

For mass cytometry analysis, PBMCs collected from 20 healthy donors were frozen in 10% DMSO and 90% FCS and stored in liquid nitrogen. The day before acquisition, PBMCs were thawed, counted, and stained with Cell-ID Intercalator-Rh103 (Fluidigm, San Francisco, CA) for viability testing followed by Fc blocking reagent and a surface Ab mixture. Subsequently, cells were fixed in PBS (without calcium and magnesium) with 2% paraformaldehyde, permeabilized, barcoded using the Cell-ID 20-Plex Barcoding Kit (Fluidigm), and pooled. Samples were then transferred to methanol and stored at −20°C. On the acquisition day, cells were stained with an intracellular Ab mixture and labeled with Cell-ID Intercalator-Ir. Samples were supplemented with EQ Four Element Calibration Beads (Fluidigm) and acquired on a CyTOF 2 (Fluidigm) equipped with a SuperSampler (Victorian Airship) at an event rate <350 events/s. Samples were analyzed in one run. Abs were either obtained prelabeled from Fluidigm or conjugated with metal isotopes using Maxpar X8 Ab labeling kits (Fluidigm). FCS files were normalized and debarcoded using CATALYST (1.21.1) R package. Then, the gating and downstream analysis was done in CytoExploreR (1.10) and Metagate (0.8.0) (13).

scRNA-seq data

PBNK subset scRNA-seq data originate from PBMCs isolated from one conventional NK cell donor and one adaptive NK cell donor that were subset sorted and sequenced as previously described (14). A total of 12,000 cells were directly sorted into Eppendorf tubes at 4°C for each sample using a FACSAria II (Beckton Dickinson). For both donors we sorted $CD56^{bright}$, $CD56^{dim}$ $NKG2A^+$ KIR^- $CD57^-$, $CD56^{dim}$ $NKG2A^-$ self KIR^+ $CD57^-$, and $CD56^{dim}$ $NKG2A^-$ nonself KIR^+ $CD57^-$ populations. For the adaptive donor we also sorted a population of $CD56^{dim}$ $NKG2A^+$ self-KIR^+ $CD57^+$ $NKG2C^+$ cells, and for the nonadaptive donor a population of $CD56^{dim}$ $NKG2A^-$ self-KIR^+ $CD57^+$ NK cells. For the Abs, CD57-FITC (HNK-1) was from BioLegend; KIR3DL1S1-allophycocyanin (Z27.3.7), CD56-ECD (N901), and CD158b1/b2,j-PE-Cy5.5 (GL183) were from Beckman Coulter; KIR2DL1-allophycocyanin-Cy7 (REA284), NKG2C-PE (REA205), and NKG2A-PE 463 Vio770 (REA110) were from Miltenyi Biotec. These data are available at GEO with accession number GSE245690. The scRNA-seq data from IL-15–stimulated cells were previously published, and the raw data are available at EGA under accession number EGAS00001003946 (15). The data from after target stimulation are taken from Dufva et al. (16).

scRNA-seq analysis

The scRNA-seq data were analyzed using Scanpy (17). After filtering and quality control, the remaining cells were analyzed using scANVI (18) with the known subset membership as label annotations. Uniform manifold approximation and projection for dimension reduction (UMAP) embeddings were computed on the latent scANVI representations. For the unstimulated PBNK cell data and the data from after target stimulation, the resulting denoised RNA expression value for *ADGRG1* was plotted on the UMAP embeddings. The dot plots showing the expression of *ADGRG1* across the subsets and conditions were made with the merged dataset of all relevant donors.

Small interfering RNA silencing

We performed knockdown according to a previously published protocol (19). In short, isolated NK cells were counted and washed in prewarmed PBS. Then, cells were resuspended at a concentration of 1×10^6 cells/ml in prewarmed Accel siRNA (small interfering RNA) delivery medium (Horizon Discovery) supplemented with penicillin/streptomycin and 1 ng/ml IL-15 from Miltenyi Biotec. A total of 100 μl cells/well (1×10^5 cells) was seeded in a U-bottom 96-well plate. Finally, Accell human ADGRG1 siRNA was added at a final concentration of 1 μM, and 1 μM Accell Non-targeting siRNA was added to another well as a control (Horizon Discovery). Cells were incubated at 37°C for 96 h before use. The media were not changed during the 96-h incubation. For subsequent experiments, NK cells were washed and resuspended in complete RPMI and used immediately after the 96 h.

Transwell migration assays

A total of 5×10^5 purified primary PBNK cells rested overnight in complete RPMI were seeded in the top well of 5-μm polycarbonate pore transwell plates (Corning). The bottom well was filled until it touched the transwell membrane with complete RPMI with or without 10 ng/ml rIL-8 (PeproTech). Primary NK cells were prepared, either preincubated with or without purified unconjugated anti-GPR56 (CG4; BioLegend) Ab 5 μg/ml for 1 h at 37°C or treated with nontargeting siRNA or GPR56 siRNA according to the earlier protocol. Plates were incubated at 37°C at 5% CO_2 for 1 h. After the incubation, CountBright counting beads (Thermo Fisher) were added to the bottom well. All the cells and beads were collected from the bottom well and stained for subsequent flow cytometry analysis and counting. Cell counts in transwell assays were normalized based on the CountBright beads' manufacturer: $\left(\frac{\text{Number of cells acquired}}{\text{Beads acquired}}\right) \times \left(\frac{\text{Concentration of beads}}{\text{Volume acquired}}\right)$. Using the normalized cell counts, we calculated the migration index by: $\frac{\text{Normalized cell count of conditioned media or knockdown}}{\text{Normalized cell count in unstimulated control}}$. Statistical significance was calculated using a paired *t* test.

IL-15 stimulation

To study the GPR56 receptor dynamics in the presence of IL-15, we added 1×10^5 purified PBNK cells to 96-well plates in complete RPMI. IL-15 from Miltenyi Biotec was added to each well to a final concentration of 10 ng/ml in a time-wise manner: 2 h, 4 h, 8 h, overnight, and a control without stimulation. Finally, PBNK cells were stained with a mixture of fluorescently labeled Abs for flow cytometry analysis.

Receptor internalization

To study internalization of GPR56 with flow cytometry, we used purified anti-GPR56 Ab (CG4) that was biotinylated using the Mix-n-Stain Biotin Ab Labeling Kit (Sigma-Aldrich). Purified PBNK cells were stimulated with biotinylated anti-GPR56 Ab at a 5 μg/ml final concentration for 1 h at 37°C. The cells were then washed twice with staining buffer and incubated with Streptavidin Alexa Fluor 568 from Jackson ImmunoResearch at 4°C for 20 min. For imaging experiments, purified NK cells were stimulated with

anti-CG4 Ab or anti-DNAM1 Ab (as positive control) both at a final concentration of 5 μg/ml for 1 h, surface stained with wheat germ agglutinin (WGA) tagged with Alexa Fluor 488 for 15 min at room temperature, and allowed to adhere on Cell-Tak coated glass coverslips. Paraformaldehyde-fixed cells were permeabilized with Triton X-100, stained with Alexa Fluor 568 secondary Abs, and counterstained with Hoechst 33342. Z-stack images of the cells were acquired on LSM880 confocal microscope (Zeiss) using 63× oil-immersion objective. The number of green puncta (GPR56, DNAM1) and WGA puncta were quantified using Fiji software.

Actin remodeling

To investigate the effect of anti-GPR56 stimulation on actin filaments and the spreading/elongation of cells, we used purified PBNK cells that were rested overnight after isolation, incubated for 30 min in the presence or absence of 100 μM/ml Rho-associated protein kinase (ROCK) inhibitor Y-27632 from STEMCELL Technologies, and then stimulated with 5 μg/ml anti-GPR56 Ab for 1 h. The CG4-stimulated cells were allowed to adhere on Cell-Tak coated coverslips, whereas the unstimulated cells were plated on 5 μg/ml CD45 or CD16 Ab-coated coverslips to serve as positive and negative controls for cell spreading. Cells stimulated with soluble anti-CD45 or anti-CD16 and then plated on Cell-Tak coated coverslips also had the same effect as the control conditions using plate-bound stimulation. Cells were incubated for 60 min, fixed with 4% paraformaldehyde at room temperature, and permeabilized with 0.1% TritonX-100 for 5 min. Filamentous actin was stained with Alexa Fluor 488–tagged Phalloidin (A12379; 1:200 dilution, 30 min; Thermo Fisher Scientific) and counterstained with Hoechst 33342 (62249; 1:2000 dilution, 5 min; Thermo Fisher Scientific). Z-stack images of the cells were acquired on LSM880 confocal microscope (Zeiss) on 63× oil-immersion objective, and area, length, and breadth were quantified using Fiji software. Phalloidin staining served to mark the cell boundaries; the longest straight line through the nucleus was taken as the length, whereas the shortest perpendicular line through the nucleus was taken as breadth.

Detection of GPR56 at the leading edge of migrating NK cells

NK cells were rested overnight in RPMI medium without IL-15, and 20,000 cells were added to 0.01% poly-L-lysine solution–coated coverslips that were placed in a 24-well plate. Cells were stimulated with 5 μg/ml anti-GPR56 Ab (CG4 clone, 358202; BioLegend) in CO_2 incubator for 1 h. Cells were fixed with 4% formaldehyde for 15 min and permeabilized with 0.01% saponin in PBS for 5 min. Filamentous actin was stained by Alexa Fluor 555–tagged Phalloidin (A34055; 1:200 dilution; Thermo Fisher Scientific), and GPR56 was stained with Alexa Fluor 488–tagged anti-mouse secondary Ab for 1 h at room temperature. The nucleus was stained with Hoechst (1:2000 dilution in PBS), and cells were washed in PBS containing 0.01% Tween 20 and mounted on glass slides using Fluoromount G (Southern Biotech). Confocal images of cells were obtained using 1.4 N.A. oil immersion 63× objective of LSM880 microscope, at 4× zoom. Using Fiji software, we quantified intensity of GPR56 at the first half comprising the leading edge versus the second half comprising the trailing edge. Quantification of GPR56 from 57 NK cells in total from three donors is shown. Approximately 20 polarized cells with distinguishable leading and trailing edge (based on actin staining) were randomly selected from each donor for analysis.

Yes-associated protein-transcriptional coactivator with PDZ-binding motif nuclear translocation

To investigate Yes-associated protein (YAP)-transcriptional coactivator with PDZ-binding motif (TAZ) nuclear translocation, we stained unstimulated and 1-h anti-GPR56 (CG4)-stimulated NK cells with YAP (clone D8H1X; Cell Signaling) or TAZ (clone V386; Cell Signaling) Abs and secondary Alexa Fluor 488 Ab, Phalloidin 555 (A34055; Thermo Fisher Scientific) to stain actin, and nucleus by Hoechst 33342. YAP levels were undetectable in NK cells, whereas the ratio of nuclear versus cytosolic TAZ levels was quantified by measuring the raw integrated density (intensity over area) of TAZ signals using Fiji/Imaris software.

Results

Expression of GPR56 mRNA and protein correlates with NK cell differentiation

Previous studies have shown GPR56 protein to be preferentially expressed by the cytotoxic cells of the lymphocyte compartment, including NK cells and all populations of cytotoxic T cells (6, 11). To provide a detailed, subset-specific analysis of GPR56 expression in human NK cells, we mapped the expression of GPR56 onto a previously established human NK cell transcriptional reference map based on both sorted phenotypically defined subsets and bulk single-cell RNA sequencing (scRNAseq) data. Our analysis revealed a progressive increase in the transcripts of the GPR56 encoding gene ADGRG1 as NK cells matured from $CD56^{bright}$ to various stages of $CD56^{dim}$ NK cells, characterized by the expression of markers such as KIR, NKG2A, CD57, and NKG2C (Fig. 1A, 1B). Cell-surface protein expression of GPR56 followed the same pattern and was uniformly expressed at high levels in more differentiated stages (Fig. 1C–E). GPR56 expression on $NKG2A^{-}KIR^{+}NKG2C^{+}$ adaptive NK cells, found in some CMV^{+} donors (20), was equal or slightly higher than the most mature conventional NK cell subsets (Fig. 1F with gating scheme in Supplemental Fig. 1A, 1B). Finally, despite similar transcriptional levels, educated NK cells expressed higher levels of GPR56 than uneducated NK cells (Fig. 1G). Hence we observed higher levels of GPR56 in $KIR2DL3^{+}$ NK cells in donors homozygous for the self-ligand HLA-C1, and conversely, in $KIR2DL1^{+}$, expression was higher in donors homozygous for HLA-C2. These data corroborate and extend previous reports showing that GPR56 protein is higher in the $CD56^{dim}$ NK cell population compared with $CD56^{bright}$ (12) and especially high on memory-like $PLZF^{low}$ $FcR\gamma^{-}$ NK cells, corresponding to the adaptive $NKG2C^{+}$ NK cell population examined in this study (12).

GPR56 silencing and agonistic receptor ligation increase NK cell migration

GPR56 is a known adhesion GPCR and has been reported to influence cell migration in various cell types (21–25). In NK-92 cells, ectopic expression of GPR56 inhibited spontaneous and SDF-1–stimulated cell migration (6). We found that spontaneous migration of primary resting NK cells through a 5-μm polycarbonate transwell membrane led to a consistent downregulation of GPR56 (Fig. 2A). Because GPR56 has been reported to negatively influence NK cell function (12), we hypothesized that the dynamic downregulation of GPR56 during migration reflected a direct involvement of this receptor in the migratory behavior of NK cells. Therefore, to further delineate the role of GPR56 in primary NK cells, we silenced its expression in primary NK cells by siRNA (19) and monitored functional responses and changes in the spontaneous and chemokine-directed migratory response. In agreement with previous studies (12), successful silencing of GPR56 (Fig. 2B) was associated with an increase in the open conformation of LFA-1 and increased degranulation and cytokine production in response to target cell stimulation (Supplemental Fig. 2A–C). Notably, silencing of GPR56 led to increased spontaneous migration of primary NK cells (Fig. 2C). The enhanced migratory effect of GPR56 siRNA was seen in bulk NK cells but was most profound in the differentiated $NKG2A^{-}KIR^{+}$ $CD57^{+}$ subset of NK cells that expressed the highest baseline levels of GPR56. There was no significant effect in the $CD56^{bright}$ cells that expressed low baseline levels of GPR56. In addition, IL-8–directed migration was increased in GPR56 siRNA–treated cells compared with cells treated with control siRNA (Fig. 2C). In addition, similar results were obtained for CX3CL1 (Fractalkine)-driven migration, albeit with some more variability (Fig. 2C). In conclusion, silencing GPR56 increased both spontaneous and directed migration of NK cells, indicating a functional role of GPR56 in migration.

To further evaluate the functional role of GPR56, we stimulated NK cells with an agonistic anti-GPR56 Ab and studied its effect on migration. Prestimulation of NK cells with anti-GPR56 increased the migratory capacity of the cells similarly to GPR56 siRNA treatment and following the same subset-specific pattern (Fig. 2D). Confocal microscopy imaging of anti-GPR56–treated cells revealed that GPR56 was rapidly lost from the surface within 1 h poststimulation

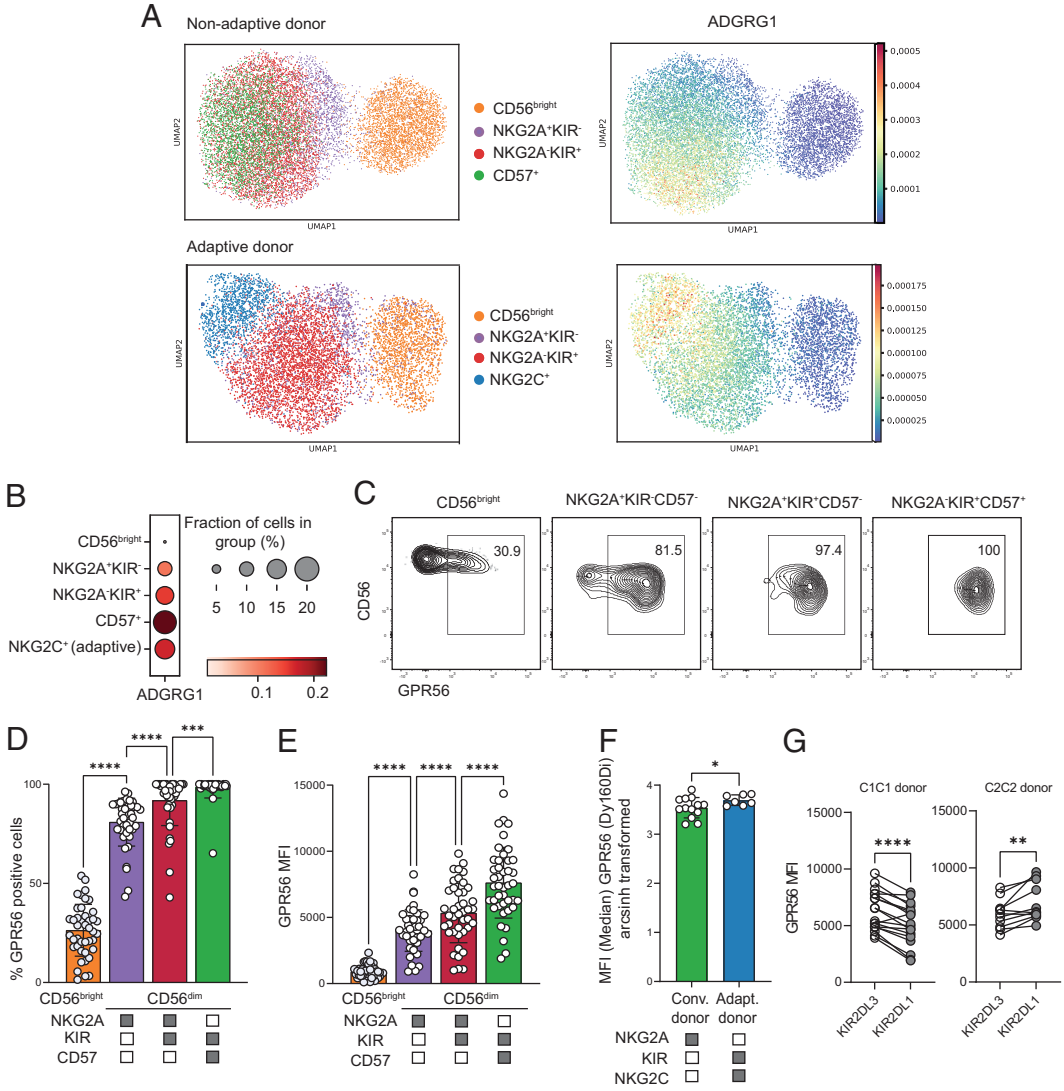

FIGURE 1. GPR56 (ADGRG1) mRNA and protein expression in NK cell subsets. (**A**) scRNAseq analysis of sorted PBNK cell subsets from two healthy blood donors, one with and one without adaptive NK cell population. Analysis performed by Scanpy (17). (**B**) Dot plot summarizing scRNAseq analysis of ADGRG1 expression in different PBNK cell subsets. (**C**) Flow density plots showing GPR56 protein expression on gated NK subsets from one representative experiment. The gating strategy of NK subsets is visualized in Supplemental Fig. 1A. (**D**) Fraction of GPR56$^+$ cells in the different NK subsets, and (**E**) GPR56 surface protein expression, analyzed by flow cytometry, and measured as % positive cells and mean fluorescence intensity (MFI) ($n = 42$). Statistics were performed with repeated measures one-way ANOVA. (**F**) GPR56 surface expression analyzed by mass cytometry and measured in MFI from conventional donors ($n = 13$) and adaptive donors ($n = 7$). The gating strategy of NK subsets is visualized in Supplemental Fig. 1B. Statistics were performed with Welch's t test. (**G**) GPR56 surface expression measured in MFI from educated and uneducated donors in single KIR-expressing NK cells from C1C1 donors ($n = 18$) and C2C2 donors ($n = 11$). Statistics were performed with paired t test. *$p \leq 0.05$, **$p \leq 0.01$, ***$p \leq 0.001$, ****$p \leq 0.0001$.

and at least partly because of its translocation to the intracellular compartment (Fig. 2E–G). The loss of surface expression was replicated in flow cytometry using the same experimental conditions (Fig. 2H). These data show that loss of surface expression of GPR56, either through siRNA silencing or through receptor ligation and internalization, is associated with increased migratory response of NK cells.

Transcriptional loss of GPR56 expression after cytokine and target cell stimulation

It is well established that cytokines, including IL-15, promote migratory responses in NK cells (26). Furthermore, it was previously reported that cell-surface expression of GPR56 in purified NK cells is sensitive to long-term (4–20 d) cytokine stimulation with IL-2 (11) and shorter stimulations (12–24 h) with IL-15 and/or IL-18 (11, 12). Therefore, we next studied the kinetics of GPR56 downregulation after various types of stimulation. We found that downregulation occurred quickly with a reduction of >50% of cell-surface GPR56 within the first 8 h after stimulation with 10 ng/ml IL-15 (Fig. 3A). This was associated with a general shutdown in ADGRG1 transcription in both NKG2A$^+$ and KIR$^+$ NK cell subsets and was seen in nonproliferating (generation 0–1) and proliferating cells (generation > 2) (Fig. 3B). Similarly, stimulation of NK cells with K562 target cells or through CD16 or DNAM/2B4 cross-linking using FcR$^+$ P815 target cells induced a profound reduction of cell-surface GPR56 (Fig. 3C, 3D). Finally, we analyzed an integrated and publicly available dataset with primary NK cells stimulated by 26 different tumor cell lines to assess how target cell stimulation affected ADGRG1 transcripts (16). We used the cell-type annotations provided by Dufva et al. and plotted ADGRG1 expression in target-induced NK cell states (type I IFN,

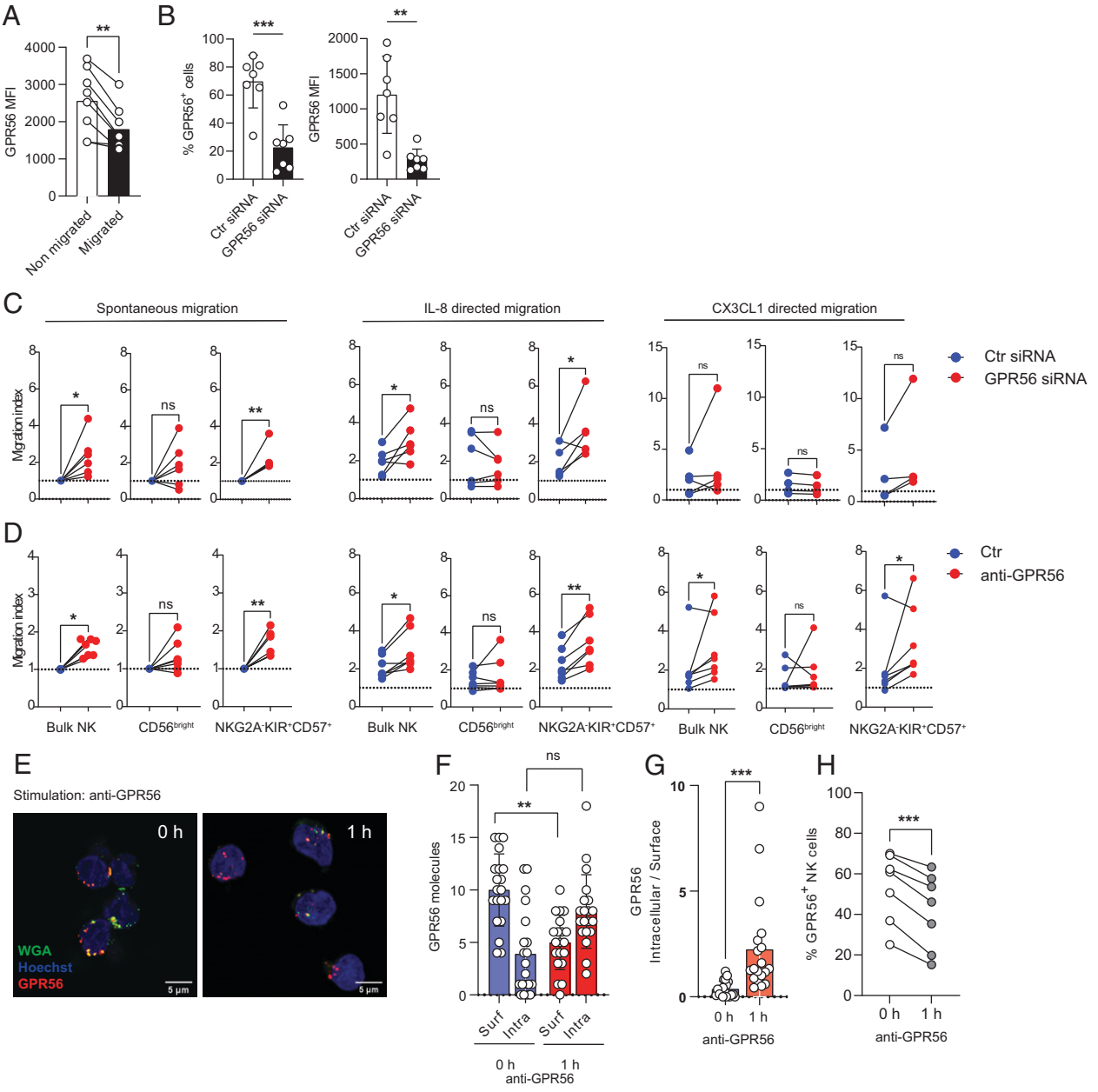

FIGURE 2. GPR56 modulates the migratory capacity of NK cells. (**A**) Cell-surface GPR56 expression measured in mean fluorescence intensity (MFI) in nonmigrated and migrated primary NK cells in a transwell setting ($n = 8$). Statistics were performed by a paired t test. (**B**) GPR56 knockdown efficiency measured in MFI and percent comparing a nontargeting siRNA control and GPR56 targeting siRNA treatment ($n = 7$). Statistics were performed using paired t test. (**C**) Spontaneous, IL-8 (10 ng/ml), and CX3CL1 (10 ng/ml) primary NK cell migration in a transwell setting in bulk NK cells, $CD56^{bright}$ NK cells, and $NKG2A^{-}KIR^{+}CD57^{+}$ NK cells comparing NK cells with a nontargeting siRNA treatment and GPR56 knockdown NK cells by siRNA ($n = 6$). Statistics were performed by a paired t test. (**D**) Spontaneous, IL-8 (10 ng/ml), and CX3CL1 (10 ng/ml) primary NK cell migration in a transwell setting in bulk NK cells, $CD56^{bright}$ NK cells, and $NKG2A^{-}KIR^{+}CD57^{+}$ NK cells comparing unstimulated NK cells and NK cells stimulated with an anti-GPR56 Ab ($n = 7$). Statistics were performed using a Wilcoxon test. (**E**) Confocal imaging of GPR56 in freshly isolated PBNKs after Ab stimulation for 1 h. Green: WGA tagged with Alexa Fluor 488. Blue: Hoechst 33342. Red: GPR56 stained with Alexa Fluor 568 secondary Abs. One representative image for 0 and 1 h from a single experiment is shown. (**F**) Counted GPR56 clusters detected in the cell surface (membrane) at 0 h versus intracellular and 1 h after stimulation with anti-GPR56 Ab ($n = 3$ donors/110 NK cells). Statistics were performed by a mixed-effects analysis. (**G**) Intracellular-to-surface ratio of GPR56 clusters ($n = 3$ donors/110 NK cells). Statistics were performed using a paired t test. (**H**) Surface expression of GPR56 was detected by flow cytometry after Ab stimulation for 0 or 1 h ($n = 7$). Statistics were performed by a paired t test. $*p \leq 0.05$, $**p \leq 0.01$, $***p \leq 0.001$.

cytokine producing, and activated) (16). We found that all responding NK cell populations showed reduced *ADGRG1* transcripts after tumor cell stimulation, supporting a transcriptional feedback loop induced by both cytokines and natural receptor ligation (Fig. 3E).

Together, these data suggest that GPR56 functions as an inhibitory checkpoint for NK cell migration, and that its transcription and surface expression decrease after agonistic receptor ligation, cytokine stimulation, and target cell recognition.

GPR56 engagement leads to actin remodeling

The Rho signaling pathway is important for immune cell migration (27). Rho belongs to the Rho family small GTPases of the Ras

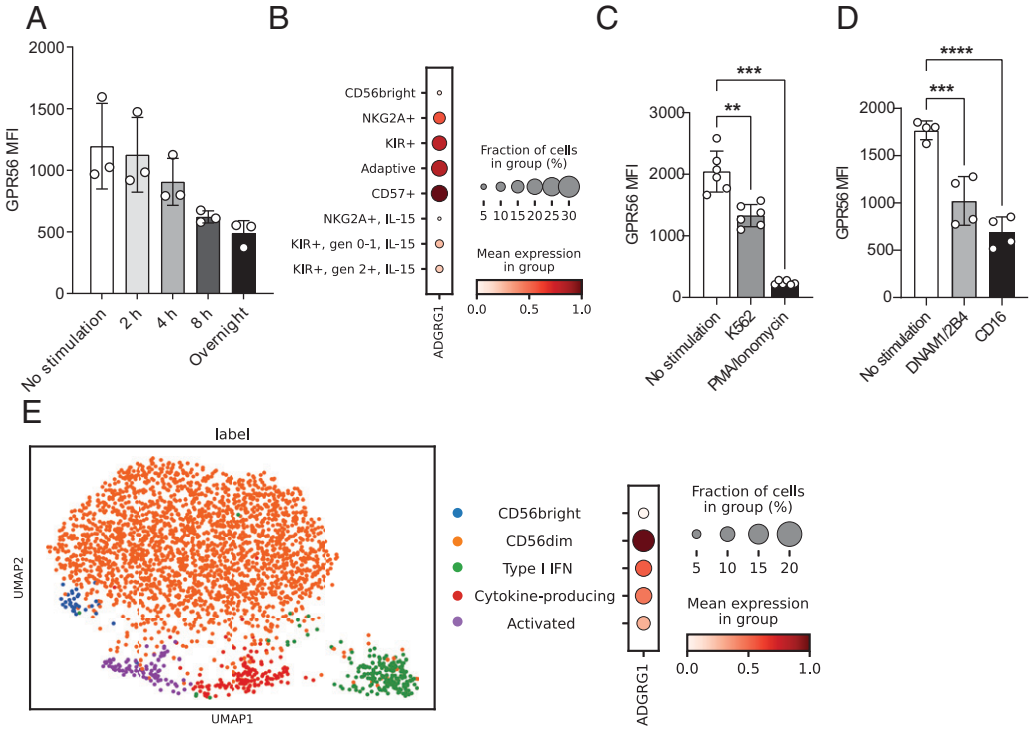

FIGURE 3. Transcriptional regulation of GPR56 expression. (**A**) Surface expression of GPR56 measured by flow cytometry upon IL-15 stimulation (10 ng/ml) at different time points ($n = 3$ donors). (**B**) Dot plot showing transcriptional levels of *ADGR1* in the indicated subset after stimulation with IL-15 for 5 d. (**C**) GPR56 surface expression upon target cell stimulation (K562) and PMA (2.5 μg/ml)/ionomycin (0.5 μg/ml) activation ($n = 6$). Statistics were performed using repeated measures one-way ANOVA. (**D**) GPR56 surface expression measured as MFI upon stimulation with DNAM1/2B4 and CD16 using a P815 cell line in a reverse Ab-dependent cytotoxicity assay. (**E**) UMAP representing the CD56^{bright} and CD56^{dim} compartment and the clusters induced by target cell stimulation with the dot plot showing the relative *ADGRG1* transcripts in the indicated clusters. Statistics were performed using repeated measures one-way ANOVA ($n = 4$). $^{ns}p > 0.05$, $^{**}p \leq 0.01$, $^{***}p \leq 0.001$, $^{****}p \leq 0.0001$.

superfamily that in a GTP-bound active state can bind and activate several downstream effector molecules (28), with one of these being ROCK. To investigate whether Rho/ROCK signaling is involved in GPR56-induced migration, we stimulated cells with anti-GPR56 Ab and evaluated the induced changes in the actin filament network in the absence and presence of ROCK inhibitor (Fig. 4A–C). Within 1 h of stimulation with anti-GPR56 Ab, we observed distinct remodeling of the actin filaments and the shape of the cells, visualized by phalloidin staining of filamentous F-actin (Fig. 3A). GPR56-stimulated NK cells displayed increased surface area and were elongated compared with NK cells stimulated with anti-CD45 as negative control (Fig. 4B, 4C). Anti-CD16 stimulation was included as a positive control to evaluate the effect of cell migration on cellular area and elongation, and its dependence on Rho/ROCK signaling. In all conditions, actin remodeling was inhibited in the presence of ROCK inhibitor.

GPR56 is located near the leading edge and its downmodulation triggers TAZ translocation

One of the key hallmarks of cell migration is the formation of the leading edge and mechanistic adhesion after actin polymerization (29, 30). To determine the physical location of GPR56 on migrating NK cells, we treated primary NK cells with an anti-GPR56 Ab leading to a migratory phenotype as described earlier. Through confocal microscopy, GPR56 expression was detected preferentially at the leading edge of the cell (Fig. 4D, 4E), consistent with a role in NK cell migration.

YAP or its paralogue TAZ in their active form translocate to the nucleus and associate with the family of TEA domain transcription factors (TEAD) to regulate several processes, such as cell proliferation, tissue growth, and differentiation (31). YAP/TAZ is also shown to limit cytoskeletal tension, which is important for persistent cell motility (32). To investigate whether GPR56 receptor stimulation and subsequent actin polymerization induce nuclear translocation of YAP/TAZ, we isolated primary NK cells, stimulated them with anti-GPR56 Ab, and imaged by confocal microscopy. TAZ was translocated to the nucleus after 1-h stimulation (Fig. 4F, 4G), indicating that GPR56 stimulation relays signals that enable persistent migratory capability of the NK cells. We were not able to detect any staining of YAP in our assays, consistent with negligible levels of YAP transcripts in NK cell RNA sequencing data (14).

Discussion

We report a role for GPR56 as an inhibitory checkpoint for spontaneous and chemokine-driven NK cell migration. Agonistic stimulation of GPR56 led to a rapid internalization and loss of surface expression unleashing a migratory phenotype that was mechanistically linked to TAZ nuclear translocation and increased actin polymerization. GPR56 expression increased with NK cell differentiation and reached its peak in terminally differentiated NK cells, which was reflected in the response to GPR56 manipulation. Our study reinforces the role for GPR56 as an upstream inhibitory checkpoint regulating a broad range of functions in human NK cells, including cell migration.

GPCRs, the largest membrane receptor class with ~800 human members, are implicated in diseases such as diabetes, depression, obesity, Alzheimer's, and cancer. Activated by external signals, they trigger responses such as cAMP production, calcium mobilization, and kinase phosphorylation. Their seven-transmembrane domain links G protein signaling to external stimuli. In immunity, GPCRs,

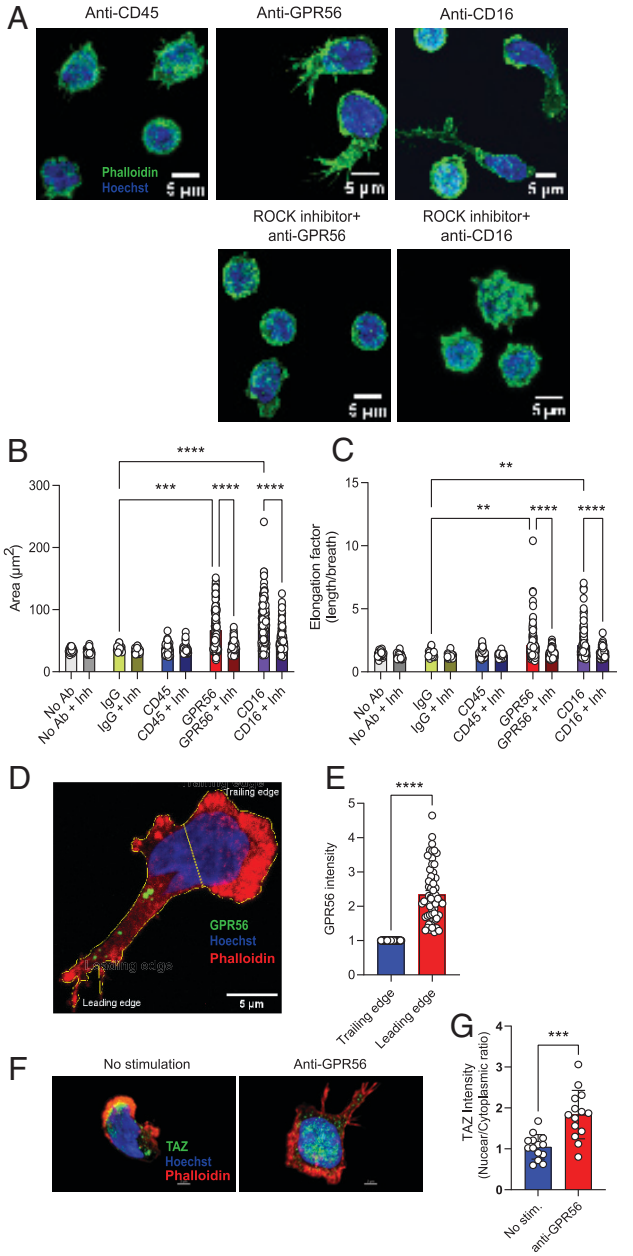

FIGURE 4. GPR56 is involved in Rho-dependent actin remodeling and translocation of TAZ. (**A**) Confocal microscopy of freshly isolated NK cells stimulated with anti-GPR56 for 1 h in the presence or absence of 100 µM/ml ROCK inhibitor. Cells were stimulated with anti-CD45 and anti-CD16 as negative and positive control, respectively. Actin filaments were stained by Phalloidin AF 488 (green), and cell nuclei were stained with Hoechst 33342 (blue). One representative image for each setting from a single experiment is shown. (**B**) Actin remodeling is visualized by the flattening over an area (measured by μm^2). Average cell area from all cells present in the view field; total 10–11 view fields ($n = 3$ donors). Statistics were performed using Kruskal-Wallis multiple comparisons test. (**C**) The elongation factor (cell length/breadth) of the cells described in (B). Statistics were performed using Kruskal-Wallis multiple comparisons test. (**D**) Representative image of an NK cell with a clear leading edge and trailing edge showing GPR56 in green and F-actin in red. (**E**) GPR56 intensity ratio comparing GPR56 clusters in the trailing edge and leading edge ($n = 3$ donors). Total cells analyzed = 57. Statistics were performed using a paired *t* test. (**F**) Stimulation with anti-GPR56 for 1 h induces nuclear translocation of TAZ. Actin filaments were visualized with Phalloidin AF555 and nuclei with Hoechst 33342. Translocation was measured as the ratio of nuclear/cytoplasmic TAZ intensity. (**G**) TAZ expression intensity within the nucleus/cytoplasmatic comparing unstimulated versus anti-GPR56 treatment for 1 h ($n = 3$ donors). Each dot represents TAZ intensity per view field. Statistics were performed using unpaired *t* test. $^{**}p \leq 0.01$, $^{***}p \leq 0.001$, $^{****}p \leq 0.0001$.

especially chemokine receptors, regulate cell migration and homing (33). Adhesion GPCRs have a large N-terminal domain for cell interactions and a conserved GPCR autoproteolysis-inducing (GAIN) domain, undergoing proteolysis to produce an N-terminal fragment (NTF) and a C-terminal fragment (CTF) with a tethered agonist. Postcleavage, NTF and CTF remain associated, affecting cell adhesion and signaling (34). Immune cells express adhesion GPCRs, including EMR, EMR2, and CD97, which are crucial for immune tolerance, neutrophil recruitment, and leukocyte trafficking (35–37).

The role of GPR56 in regulating migration is well established in various cell types, including neural progenitor and melanoma cells. GPR56 deficiency causes bilateral frontoparietal polymicrogyria, a brain disorder (38). In cervical cancer, high GPR56 levels predict poor outcomes, whereas its suppression reduces cell proliferation (39). GPR56 activation, using an agonistic mAb, in melanoma cells enhanced invasion and migration (24). These variable response patterns may be because of the presence/absence of *cis*-acting coreceptors able to modulate receptor activity or tissue-specific splice variants (40). Indeed, a functional splice variant of GPR56 lacking the proteolytic GAIN domain has been reported in cervix, colon, leukocyte, and thyroid gland (41). In terms of GPR56 activation models, these include shedding its NTF domain, enabling receptor signaling, and interactions with membrane proteins such as CD81 and CD9. In NK cells, GPR56 signaling inhibits functional activity via a physical interaction with CD81, independent of GAIN domain cleavage (12). It has previously been shown that the NTF of GPR56 also can be shed from the cell surface in an a disintegrin and metalloprotease 17–independent manner (12). Thus, although we observed a rapid internalization of GPR56 after agonistic receptor stimulation, we cannot exclude shedding as a parallel mechanism partly responsible for the loss of GPR56 surface expression paralleling the emergence of a migratory phenotype.

Somewhat paradoxically, both genetic silencing and agonistic stimulation were associated with an unleashed NK cell migratory response. Although the detailed chain of events connecting agonistic receptor input to increased migration remains elusive, anti-GPR56 treatment led to a rapid and sustained loss of GPR56 expression at the surface, mimicking the siRNA-induced phenotype. We found that this phenotype is further reinforced by shutdown of transcription. We speculate that the extracellular N terminus of GPR56 acts as a hook anchoring the NK cells to the extracellular matrix or neighboring cells. When there is autocatalysis of the N-terminal fragment (by binding to anti-GPR56 Ab) or GPR56 surface expression is low (by siRNA-mediated knockdown), this physical brake may be released, leading to higher cell migration. However, further studies are needed to elucidate the exact mechanism of how surface expression of GPR56 interferes with cell migration.

Lending some mechanistic insights, our findings indicate that GPR56 regulates NK cell migration through the YAP/TAZ pathway and actin remodeling. The receptor's expression at the leading edge of migrating cells and its interaction with proteins such as α-actinin align with its role in cell adhesion and migration. TAZ has been reported to favor cell migration when it is translocated to the nucleus, as is the case for lung cancer cells (42), breast cancer cells (43), and melanoma cells (44). In our experiments, we observed that when using an anti-GPR56 Ab, the YAP/TAZ pathway is activated, resulting in a rapid translocation of TAZ to the nucleus associated with the migratory phenotype. Furthermore, GPR56 manipulation was associated with actin remodeling, which is a key process for cell migration (45). We found that anti-GPR56 treatment resulted in actin remodeling in NK cells, similar to that seen after agonistic stimulation with anti-CD16 (46). Previous reports have shown that GPR56 recruits Gα proteins, which activates Ras homolog family member A (RhoA) (22). It is known that upon depletion of RhoA,

T cells lose migration polarity (47). This is in agreement with our results in which inhibiting ROCK, a downstream protein from RhoA, prevented actin polymerization after both anti-GPR56 and anti-CD16 treatment. Furthermore, GPR56 expression was detected mostly in the leading edge of cells treated with anti-GPR56 Ab, which has also been seen in glioma cells where GPR56 expression correlated with α-actinin, a protein known for its role in cell adhesion (48). This further supports the notion that GPR56 acts as an upstream checkpoint for NK cell migration that is released upon cytokine stimulation, target cell recognition, and receptor ligation.

The finding of GPR56 as an important regulator of NK cell migration has implications for NK-cell based cancer therapies. Given the inhibitory effect of GPR56 on NK cell migration and cytolytic activity, targeting this receptor could enhance NK cell infiltration into tumors and improve immunotherapy outcomes. The diverse ligands and signaling pathways associated with GPR56 present multiple avenues for therapeutic intervention. Several ligands have been described for GPR56, including collagen III (49), transglutaminase 2 (50), heparin (23), and the small-molecule agonist 3-α-DOG (51). Downstream signaling after ligand stimulation of GPR56 is shown to require autoproteolysis by the GAIN domain, resulting in dissociation of the NTF and CTF (52). Binding to the natural ligands, however, has not yet been confirmed in NK cells. The receptor's complex role across different cell types and diseases highlights the need for further research to fully understand its mechanisms and therapeutic potential.

Acknowledgments

We are grateful for the support from the Flow Cytometry Core Facility and the Advanced Light Microscopy Facility at Oslo University Hospital, Montebello, Radiumhospitalet, and the support from the Genetics Core Facility, Oslo University Hospital, South-Eastern Norway Regional Health Authority, and University of Oslo.

Disclosures

K.-J.M. is a consultant for and has received research support for unrelated studies from Fate Therapeutics, has received research support from Oncopeptides, and is a consultant at Vycellix. All relationships have been approved by Oslo University Hospital, University of Oslo, and Karolinska Institute. The other authors have no financial conflicts of interest.

References

1. Laskowski, T. J., A. Biederstädt, and K. Rezvani. 2022. Natural killer cells in antitumour adoptive cell immunotherapy. *Nat. Rev. Cancer* 22: 557–575.
2. Ran, G. H., Y. Q. Lin, L. Tian, T. Zhang, D. M. Yan, J. H. Yu, and Y. C. Deng. 2022. Natural killer cell homing and trafficking in tissues and tumors: from biology to application. *Signal Transduct. Target. Ther.* 7: 205.
3. Domagala, J., M. Lachota, M. Klopotowska, A. Graczyk-Jarzynka, A. Domagala, A. Zhylko, K. Soroczynska, and M. Winiarska. 2020. The tumor microenvironment: a metabolic obstacle to NK cells' activity. *Cancers (Basel)* 12: 3542.
4. Walzer, T., and E. Vivier. 2011. G-protein-coupled receptors in control of natural killer cell migration. *Trends Immunol.* 32: 486–492.
5. Ganesh, R. A., K. Venkataraman, and R. Sirdeshmukh. 2020. GPR56: an adhesion GPCR involved in brain development, neurological disorders and cancer. *Brain Res.* 1747: 147055.
6. Peng, Y. M., M. D. van de Garde, K. F. Cheng, P. A. Baars, E. B. Remmerswaal, R. A. van Lier, C. R. Mackay, H. H. Lin, and J. Hamann. 2011. Specific expression of GPR56 by human cytotoxic lymphocytes. *J. Leukoc. Biol.* 90: 735–740.
7. Rao, T. N., J. Marks-Bluth, J. Sullivan, M. K. Gupta, V. Chandrakanthan, S. R. Fitch, K. Ottersbach, Y. C. Jang, X. Piao, R. N. Kulkarni, et al. 2015. High-level Gpr56 expression is dispensable for the maintenance and function of hematopoietic stem and progenitor cells in mice. *Stem Cell Res.* 14: 307–322.
8. Truong, K. L., S. Schlickeiser, K. Vogt, D. Boës, K. Stanko, C. Appelt, M. Streitz, G. Grütz, N. Stobutzki, C. Meisel, et al. 2019. Killer-like receptors and GPR56 progressive expression defines cytokine production of human CD4(+) memory T cells. *Nat. Commun.* 10: 2263.
9. Liu, C., T. Liu, Y. Hu, X. Zeng, X. Alimu, S. Song, S. Lu, Y. Song, and P. Wang. 2023. G protein-coupled receptor 56 characterizes CTLs and reflects the progression of lung cancer patients. *J. Immunol.* 211: 683–692.
10. Bilemjian, V., M. R. Vlaming, J. Álvarez Freile, G. Huls, M. De Bruyn, and E. Bremer. 2022. The novel immune checkpoint GPR56 is expressed on tumor-infiltrating lymphocytes and selectively upregulated upon TCR signaling. *Cancers*14: 3164.
11. Della Chiesa, M., M. Falco, S. Parolini, F. Bellora, A. Petretto, E. Romeo, M. Balsamo, M. Gambarotti, F. Scordamaglia, G. Tabellini, et al. 2010. GPR56 as a novel marker identifying the CD56dull CD16+ NK cell subset both in blood stream and in inflamed peripheral tissues. *Int. Immunol.* 22: 91–100.
12. Chang, G. W., C. C. Hsiao, Y. M. Peng, F. A. Vieira Braga, N. A. Kragten, E. B. Remmerswaal, M. D. van de Garde, R. Straussberg, G. M. König, E. Kostenis, et al. 2016. The adhesion G protein-coupled receptor GPR56/ADGRG1 is an inhibitory receptor on human NK cells. *Cell Rep.* 15: 1757–1770.
13. Ask, E. H., A. Tschan-Plessl, H. J. Hoel, A. Kolstad, H. Holte, and K. J. Malmberg. 2024. MetaGate: interactive analysis of high-dimensional cytometry data with metadata integration. *Patterns (N Y)* 5: 100989.
14. Netskar, H., A. Pfefferle, J. P. Goodridge, E. Sohlberg, O. Dufva, S. A. Teichmann, D. Brownlie, J. Michaëlsson, N. Marquardt, T. Clancy, et al. 2024. Pan-cancer profiling of tumor-infiltrating natural killer cells through transcriptional reference mapping. *Nat. Immunol.* 25: 1445–1459.
15. Pfefferle, A., B. Jacobs, H. Netskar, E. H. Ask, S. Lorenz, T. Clancy, J. P. Goodridge, E. Sohlberg, and K. J. Malmberg. 2019. Intra-lineage plasticity and functional reprogramming maintain natural killer cell repertoire diversity. *Cell Rep.* 29: 2284–2294.e4.
16. Dufva, O., S. Gandolfi, J. Huuhtanen, O. Dashevsky, H. Duàn, K. Saeed, J. Klievink, P. Nygren, J. Bouhlal, J. Lahtela, et al. 2023. Single-cell functional genomics reveals determinants of sensitivity and resistance to natural killer cells in blood cancers. *Immunity* 56: 2816–2835.e13.
17. Wolf, F. A., P. Angerer, and F. J. Theis. 2018. SCANPY: large-scale single-cell gene expression data analysis. *Genome Biol.* 19: 15.
18. Xu, C., R. Lopez, E. Mehlman, J. Regier, M. I. Jordan, and N. Yosef. 2021. Probabilistic harmonization and annotation of single-cell transcriptomics data with deep generative models. *Mol. Syst. Biol.* 17: e9620.
19. Palacios, D., P. Momayyezi, O. Huhn, E. H. Ask, J. Dunst, K. J. Malmberg, and Q. Hammer. 2022. An optimized platform for efficient siRNA delivery into human NK cells. *Eur. J. Immunol.* 52: 1190–1193.
20. Lopez-Vergès, S., J. M. Milush, B. S. Schwartz, M. J. Pando, J. Jarjoura, V. A. York, J. P. Houchins, S. Miller, S.-M. Kang, P. J. Norris, et al. 2011. Expansion of a unique $CD57^{+}NKG2C^{hi}$ natural killer cell subset during acute human cytomegalovirus infection. *Proc. Natl Acad. Sci. USA* 108: 14725–14732.
21. Chiang, N. Y., C. C. Hsiao, Y. S. Huang, H. Y. Chen, I. J. Hsieh, G. W. Chang, and H. H. Lin. 2011. Disease-associated GPR56 mutations cause bilateral frontoparietal polymicrogyria via multiple mechanisms. *J. Biol. Chem.* 286: 14215–14225.
22. Ackerman, S. D., C. Garcia, X. Piao, D. H. Gutmann, and K. R. Monk. 2015. The adhesion GPCR Gpr56 regulates oligodendrocyte development via interactions with $G\alpha_{12/13}$ and RhoA. *Nat. Commun.* 6: 6122.
23. Chiang, N. Y., G. W. Chang, Y. S. Huang, Y. M. Peng, C. C. Hsiao, M. L. Kuo, and H. H. Lin. 2016. Heparin interacts with the adhesion GPCR GPR56, reduces receptor shedding, and promotes cell adhesion and motility. *J. Cell. Sci.* 129: 2156–2169.
24. Chiang, N. Y., Y. M. Peng, H. H. Juang, T. C. Chen, H. L. Pan, G. W. Chang, and H. H. Lin. 2017. GPR56/ADGRG1 activation promotes melanoma cell migration via NTF dissociation and CTF-mediated $G\alpha_{12/13}$/RhoA signaling. *J. Invest. Dermatol.* 137: 727–736.
25. Singer, K., R. Luo, S. J. Jeong, and X. Piao. 2013. GPR56 and the developing cerebral cortex: cells, matrix, and neuronal migration. *Mol. Neurobiol.* 47: 186–196.
26. Allavena, P., G. Giardina, G. Bianchi, and A. Mantovani. 1997. IL-15 is chemotactic for natural killer cells and stimulates their adhesion to vascular endothelium. *J. Leukoc. Biol.* 61: 729–735.
27. Biro, M., M. A. Munoz, and W. Weninger. 2014. Targeting Rho-GTPases in immune cell migration and inflammation. *Br. J. Pharmacol.* 171: 5491–5506.
28. Mosaddeghzadeh, N., and M. R. Ahmadian. 2021. The RHO family GTPases: mechanisms of regulation and signaling. *Cells* 10: 1831.
29. Dupré, L., R. Houmadi, C. Tang, and J. Rey-Barroso. 2015. T lymphocyte migration: an action movie starring the actin and associated actors. *Front. Immunol.* 6: 586.
30. Petrie, R. J., and K. M. Yamada. 2012. At the leading edge of three-dimensional cell migration. *J. Cell. Sci.* 125: 5917–5926.
31. Totaro, A., T. Panciera, and S. Piccolo. 2018. YAP/TAZ upstream signals and downstream responses. *Nat. Cell. Biol.* 20: 888–899.
32. Mason, D. E., J. M. Collins, J. H. Dawahare, T. D. Nguyen, Y. Lin, S. L. Voytik-Harbin, P. Zorlutuna, M. C. Yoder, and J. D. Boerckel. 2019. YAP and TAZ limit cytoskeletal and focal adhesion maturation to enable persistent cell motility. *J. Cell. Biol.* 218: 1369–1389.
33. Lachota, M., K. Zielniok, D. Palacios, M. Kanaya, L. Penna, H. J. Hoel, M. T. Wiiger, L. Kveberg, W. Hautz, R. Zagożdżon, and K. J. Malmberg. 2023. Mapping the chemotactic landscape in NK cells reveals subset-specific synergistic migratory responses to dual chemokine receptor ligation. *EBioMedicine* 96: 104811.
34. Stoveken, H. M., A. G. Hajduczok, L. Xu, and G. G. Tall. 2015. Adhesion G protein-coupled receptors are activated by exposure of a cryptic tethered agonist. *Proc. Natl Acad. Sci. USA* 112: 6194–6199.
35. Hamann, J., B. Vogel, G. M. van Schijndel, and R. A. van Lier. 1996. The seven-span transmembrane receptor CD97 has a cellular ligand (CD55, DAF). *J. Exp. Med.* 184: 1185–1189.
36. van den Berg, T. K., and G. Kraal. 2005. A function for the macrophage F4/80 molecule in tolerance induction. *Trends Immunol.* 26: 506–509.
37. Yona, S., H. H. Lin, P. Dri, J. Q. Davies, R. P. Hayhoe, S. M. Lewis, S. E. Heinsbroek, K. A. Brown, M. Perretti, J. Hamann, et al. 2008. Ligation of the adhesion-GPCR EMR2 regulates human neutrophil function. *FASEB J.* 22: 741–751.
38. Piao, X., R. S. Hill, A. Bodell, B. S. Chang, L. Basel-Vanagaite, R. Straussberg, W. B. Dobyns, B. Qasrawi, R. M. Winter, A. M. Innes, et al. 2004. G protein-

coupled receptor-dependent development of human frontal cortex. *Science* 303: 2033–2036.
39. Zhang, S., K. Guo, Y. Liang, K. Wang, S. Liu, and X. Yang. 2021. ADGRG1 is a predictor of chemoresistance and poor survival in cervical squamous carcinoma. *Front. Oncol.* 11: 671895.
40. Huang, K. Y., and H. H. Lin. 2018. The activation and signaling mechanisms of GPR56/ADGRG1 in melanoma cell. *Front. Oncol.* 8: 304.
41. Bjarnadóttir, T. K., K. Geirardsdóttir, M. Ingemansson, M. A. Mirza, R. Fredriksson, and H. B. Schiöth. 2007. Identification of novel splice variants of adhesion G protein-coupled receptors. *Gene* 387: 38–48.
42. Han, T., J. Gao, L. Wang, Y. Qu, A. Sun, K. Peng, J. Zhu, H. Liu, W. Yang, G. Shao, and Q. Lin. 2020. ASK1 inhibits proliferation and migration of lung cancer cells via inactivating TAZ. *Am. J. Cancer Res.* 10: 2785–2799.
43. Chan, S. W., C. J. Lim, K. Guo, C. P. Ng, I. Lee, W. Hunziker, Q. Zeng, and W. Hong. 2008. A role for TAZ in migration, invasion, and tumorigenesis of breast cancer cells. *Cancer Res.* 68: 2592–2598.
44. Miao, Y., W. Zhang, S. Liu, X. Leng, C. Hu, and H. Sun. 2021. HOXC10 promotes growth and migration of melanoma by regulating Slug to activate the YAP/TAZ signaling pathway. *Discov. Oncol.* 12: 12.
45. Lee, B. J., E. Hegewisch Solloa, M. J. Shannon, and E. M. Mace. 2020. Generation of cell-derived matrices that support human NK cell migration and differentiation. *J. Leukoc. Biol.* 108: 1369–1378.
46. Brown, A. C., I. M. Dobbie, J. M. Alakoskela, I. Davis, and D. M. Davis. 2012. Super-resolution imaging of remodeled synaptic actin reveals different synergies between NK cell receptors and integrins. *Blood* 120: 3729–3740.
47. Heasman, S. J., L. M. Carlin, S. Cox, T. Ng, and A. J. Ridley. 2010. Coordinated RhoA signaling at the leading edge and uropod is required for T cell transendothelial migration. *J. Cell. Biol.* 190: 553–563.
48. Shashidhar, S., G. Lorente, U. Nagavarapu, A. Nelson, J. Kuo, J. Cummins, K. Nikolich, R. Urfer, and E. D. Foehr. 2005. GPR56 is a GPCR that is overexpressed in gliomas and functions in tumor cell adhesion. *Oncogene* 24: 1673–1682.
49. Luo, R., Z. Jin, Y. Deng, N. Strokes, and X. Piao. 2012. Disease-associated mutations prevent GPR56-collagen III interaction. *PLoS One* 7: e29818.
50. Xu, L., S. Begum, J. D. Hearn, and R. O. Hynes. 2006. GPR56, an atypical G protein-coupled receptor, binds tissue transglutaminase, TG2, and inhibits melanoma tumor growth and metastasis. *Proc. Natl Acad. Sci. USA* 103: 9023–9028.
51. Stoveken, H. M., S. D. Larsen, A. V. Smrcka, and G. G. Tall. 2018. Gedunin- and Khivorin-derivatives are small-molecule partial agonists for adhesion G protein-coupled receptors GPR56/ADGRG1 and GPR114/ADGRG5. *Mol. Pharmacol.* 93: 477–488.
52. Zhu, B., R. Luo, P. Jin, T. Li, H. C. Oak, S. Giera, K. R. Monk, P. Lak, B. K. Shoichet, and X. Piao. 2019. GAIN domain-mediated cleavage is required for activation of G protein-coupled receptor 56 (GPR56) by its natural ligands and a small-molecule agonist. *J. Biol. Chem.* 294: 19246–19254.